Journal of Alloys and Compounds 1010 (2025) 177299

Contents lists available at ScienceDirect

Journal of Alloys and Compounds

journal homepage: www.elsevier.com/locate/jalcom

Unusual microstructure and texture transition during hot compression in an extruded Mg-Gd-Zr alloy with <0001> fiber texture

Ning Lv [a,b], Lingyu Zhao [c,*], Hong Yan [b,d], Boyu Liu [e], Rongshi Chen [b,*], Zhiwei Shan [e]

[a] School of Materials Science and Engineering, University of Science and Technology of China, 72 Wenhua Road, Shenyang 110016, China
[b] Shi-changxu Innovation Center for Advanced Materials, Institute of Metal Research, Chinese Academy of Sciences, 72 Wenhua Road, Shenyang 110016, China
[c] School of Materials Science and Engineering, Shenyang Ligong University, Shenyang 110159, China
[d] School of Materials Science and Engineering, Shandong University of Science and Technology, Qingdao, Shandong 266590, China
[e] Center for Advancing Materials Performance From the Nanoscale (CAMP-Nano) & Hysitron Applied Research Center in China (HARCC), State Key Laboratory for Mechanical Behavior of Materials, Xi'an Jiaotong University, Xi'an 710049, China

ARTICLE INFO

Keywords:
{11−21} twin
Cross-slip
Dynamic recrystallization
Texture
Mg alloys

ABSTRACT

In magnesium (Mg) alloys with high rare earth content, slip modes and twinning behaviors are quite different from that in traditional Mg alloys. Deformation mechanisms, i.e., {11−21} twinning and non-basal slips, can activate during deformation process even at room temperature (RT) and contribute effectively to microstructure and texture transition. In order to figure out the influence of temperature on these deformation mechanisms and resultant microstructure and texture transition, compression tests were conducted on an extruded Mg-17.5Gd-Zr (wt%) alloy with <0001> fiber texture at temperature range of RT-450 °C. During compression, both {10−12} and {11−21} twinning behaviors can be governed by Schmid law at RT-350 °C and act as main contributors to texture transition. When the compression tests were carried out above 400 °C, twinning behaviors almost vanished and dynamic recrystallization (DRX) preferred activating within grains with the orientation of <10–10>//compression direction. DRX changed from continuous DRX to discontinuous DRX with the temperature increasing, which can be attributed to the temperature increasing and resultant elimination of sessile structure induced by cross-slip on basal plane. DRXed grains show weak texture and the texture mainly result from the properties of several near coincident site lattice boundaries.

1. Introduction

In the past decades, magnesium (Mg) alloys had received extensive attention owing to the low density, good damping capacity and excellent recyclability [1–4]. Nevertheless, the poor formability and mechanical properties significantly restrict the wider application of Mg alloys especially in transportation and aerospace. To solve these problems, researchers have developed various Mg alloys and adding rare earth (RE) elements, i.e., gadolinium (Gd) and yttrium (Y) has been proved to be the effective method to improve the formability and mechanical properties of Mg alloys [5–7]. For example, Jiang et al. [6] fabricated extruded Mg-1.58Zn-0.52Gd (wt%) plate with a high extrusion speed of 60 m/min, which show better formability than commercial AZ31 alloy. The addition of small amount of RE elements can also promote significant ductility enhancement of the Mg alloys, which can be mainly attributed to the formation of RE texture [8].

Different from the Mg alloys with low RE content, high RE content Mg alloys, i.e., the Mg-Gd and Mg-Gd-Y based alloys, are always considered to be the ideal materials to fabricate high-strength Mg alloys owing to the excellent precipitation strengthening [9,10]. Additionally, the deformation mechanisms of Mg-RE alloys are different to the other Mg alloys [11–15]. For slip modes, the addition of RE elements can accelerate the cross-slip and double cross-slip of pyramidal <c + a> slips, which can defeat the immobilization of <c + a> dislocation induced by the pyramidal-to-basal transition [16,17], thus promote the ductility enhancement. For stacking faults, the addition of RE elements can reduced the stacking faults energy [13,14,18], thus stabilizing the dislocation on basal planes and inhabit non-planar dislocation motion, which retard the dynamic recovery [19]. For twinning behaviors, the addition of high RE content can promote the activation of {11−21} twinning due to the low sensibility of {11−21} twinning to RE solute increasing [11]. {11−21} twinning has been proved to follow the

* Corresponding authors.
E-mail addresses: lyzhao202207@sylu.edu.cn (L. Zhao), rschen@imr.ac.cn (R. Chen).

https://doi.org/10.1016/j.jallcom.2024.177299
Received 10 August 2024; Received in revised form 26 September 2024; Accepted 28 October 2024
Available online 29 October 2024
0925-8388/

Schmid law and can be influenced by the basal slip transfer condition in the twinned grains when deformed at room temperature (RT) [15,20]. However, the influence of temperature on {11−21} twinning in Mg alloy and related effect on microstructure have not been systematically investigated.

In addition, the dynamic recrystallization (DRX) in high RE content Mg alloys are still mystery. Various texture of the DRXed grains including <0001> fiber texture, basal texture and random texture can be observed in the extruded high RE content Mg alloys [15,21–23] and the influences of complex deformation modes on DRX have not been systemically investigated. Therefore, we designed compression tests operated at RT-450 °C on a <0001> fiber textured Mg-17.5Gd-Zr (wt%) alloys to show the influence of temperature on various deformation mechanisms and related microstructure transition, which will be beneficial for microstructure and texture optimization and the design of high-performance high RE content Mg alloys.

2. Experiments and methods

The extruded Mg-17.5Gd-Zr (wt%) alloys with <0001> fiber texture was used in this work. Inductively coupled plasma atomic emission spectroscopy was used to determine the compositions. The Gd content was ~17.5 (wt%) and the Zr content was < 0.1 (wt%). As shown in Fig. 1, cylindrical samples with dimensions of Φ8 × 10 mm were cut from the extruded plate and compressed along normal direction (ND) at temperature range of RT-450 °C. For microstructure and texture evolution, the compression tests were interrupted at strain of 0.2 and the strain rate was 10^{-2} s^{-1}, which is same to our previous work [20]. Before compression, samples were preheated for ~10 min. The compression tests that were conducted at RT and elevate temperature (100–450 °C) were carried out on Sans type and Instron type mechanical testing machine, respectively. After compression, the deformed specimens were sectioned in the center for electron backscatter diffraction (EBSD) observation.

Cubic specimens were cut from plate and then compressed at 400–450 °C along ND after grounding and electrolytically polishing the optical planes (Fig. 1). Compression tests were interrupted at strain of 0.1 and 0.2, and the strain rate was 10^{-2} s^{-1}. After scanning electron microscopy (SEM) observation, ion etching was carried out on the cubic specimens before EBSD observation to remove the oxide layer. Processing methods of optical planes before EBSD observation and data processing progress are same to our previous work [20]. Ion etching was carried out on Leica RES102. SEM observation was conducted on a FEI Quattro S SEM. EBSD observations were carried out on FEI Quattro S SEM and Zeiss Gemini 360 SEM equipped with EDAX-TSL EBSD system. Spherical indexing technology was used in the indexing of electron backscattered diffraction patterns.

3. Results

3.1. Initial state of the as-extruded alloy

Microstructure and texture of the as-extruded alloys were shown in Fig. 2 and fully recrystallized microstructure can be observed. As shown in Fig. 2d and e, the microstructure and inverse pole figures reveal a typical <0001> fiber texture, in which the texture components distribute uniformly along the arc between [10−10]//ND and [2−1−10]//ND. High Gd content Mg alloys usually develop a <0001> fiber texture during hot extrusion and its formation had been attributed

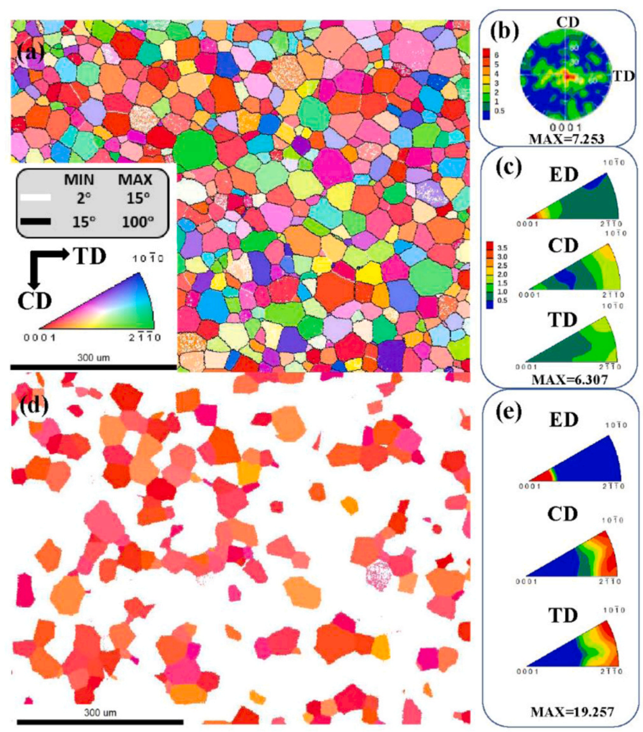

Fig. 2. Microstructure and texture of the as-extruded alloy: (a) inverse pole figure map, (b) (0001) pole figure and (c) inverse pole figures. (d) Inverse pole figure map of grains with <0001> fiber orientation and (e) related inverse pole figures.

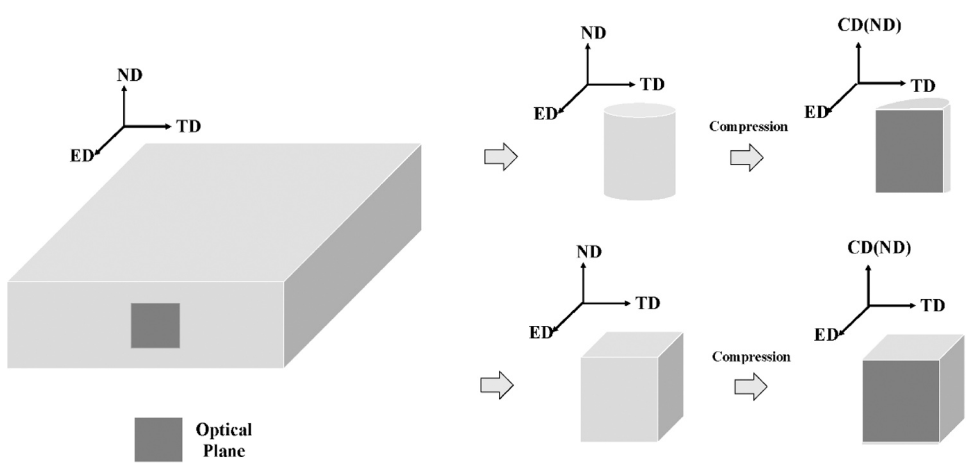

Fig. 1. Schematic illustrations of optical planes of extruded plate and compressed specimens. CD, ED and TD represent compression direction, extrusion direction and transverse direction, respectively.

to the preferential grain growth of the grains with c-axis//ED orientation [24,25].

3.2. Texture transition during compression

Textures of the compressed samples are show in Fig. 3. When compressed at the temperature below 350 °C, the <0001> fiber components almost vanished and poles which tilt from ED to CD for ~30° and ~90° appeared, which indicate that twinning behaviors can be governed by Schmid law and act as the main contributor to texture transition according to our previous work [20]. When compressed at temperature above 350 °C, the <0001> fiber components were weakened and there are no strong components whose c-axes parallel to CD formed. Interestingly, as shown in Fig. 3, <2–1–10>//CD (<10–10>//TD) components formed in all compressed samples and it can be concluded from the inverse pole figures of <0001> fiber components that such a texture in the compressed samples were induced by the consumption of the components which show <0001> fiber orientations and with <2–1–10>//CD (Fig. S1).

Misorientation angle distribution of compressed specimens were shown in Fig. 4. When compressed at RT-350 °C, peaks at 0–10°, 30–40°, 50–60° and 80–90° can be observed. The peaks at 0–10° represent the low angle grain boundaries (LAGBs) and the axis/angle distribution of other abovementioned peaks are shown in Fig. 4c-k. Extension twins including {11−21} twin (34°, [10−10]) and {10−12} twin (86°, [11–20]) can be identified. Moreover, frequent twin-twin intersection, i. e., {10−12} twin variants intersections (60°, [10−10]) can be identified. When compressed at RT-300 °C (Fig. 4c–h), the peaks which

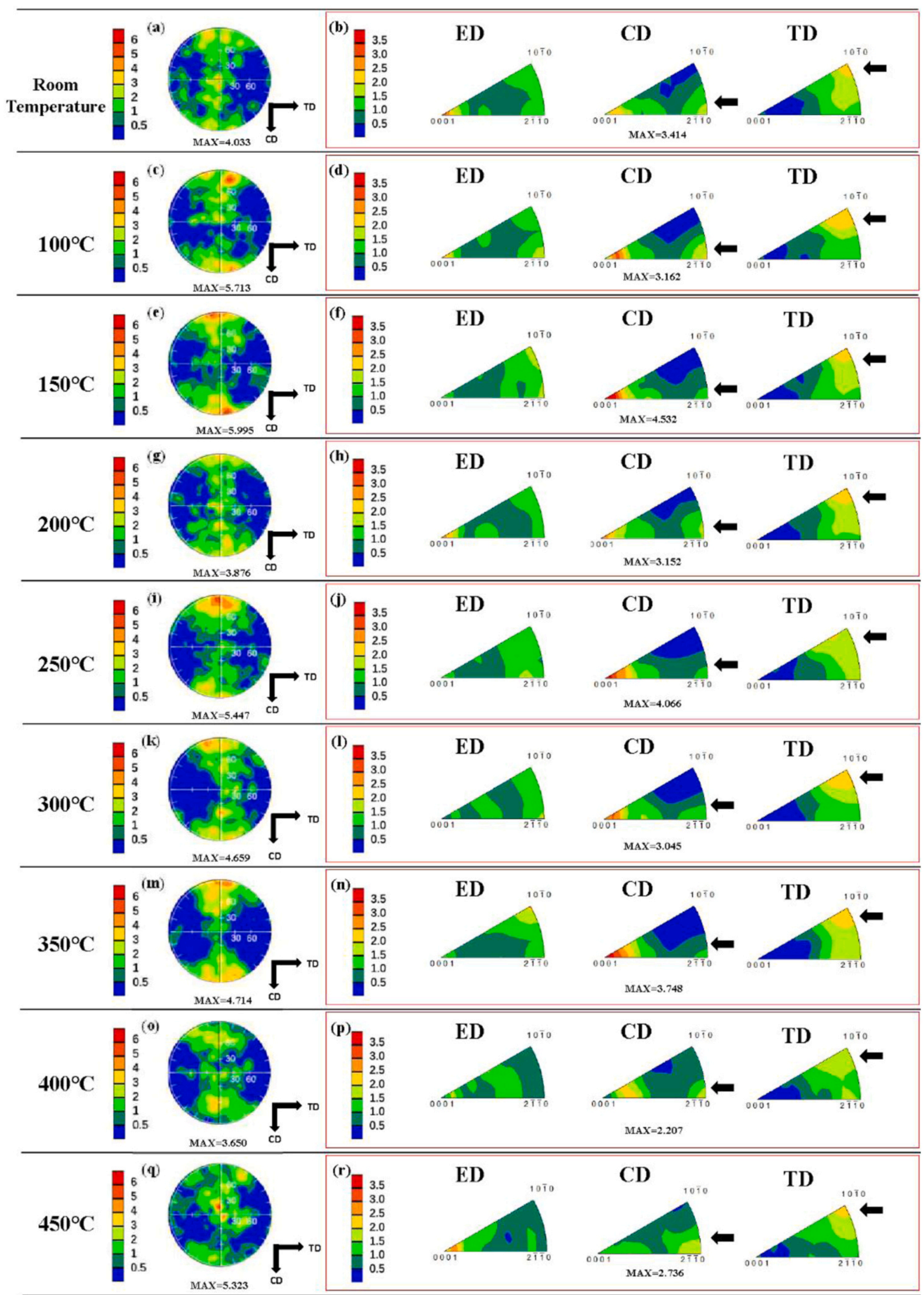

Fig. 3. . (0001) pole figures (a, c, e, g, i, k, m, o, q) and corresponding (b, d, f, h, j, l, n, p, r) inverse pole figures of the compressed samples.

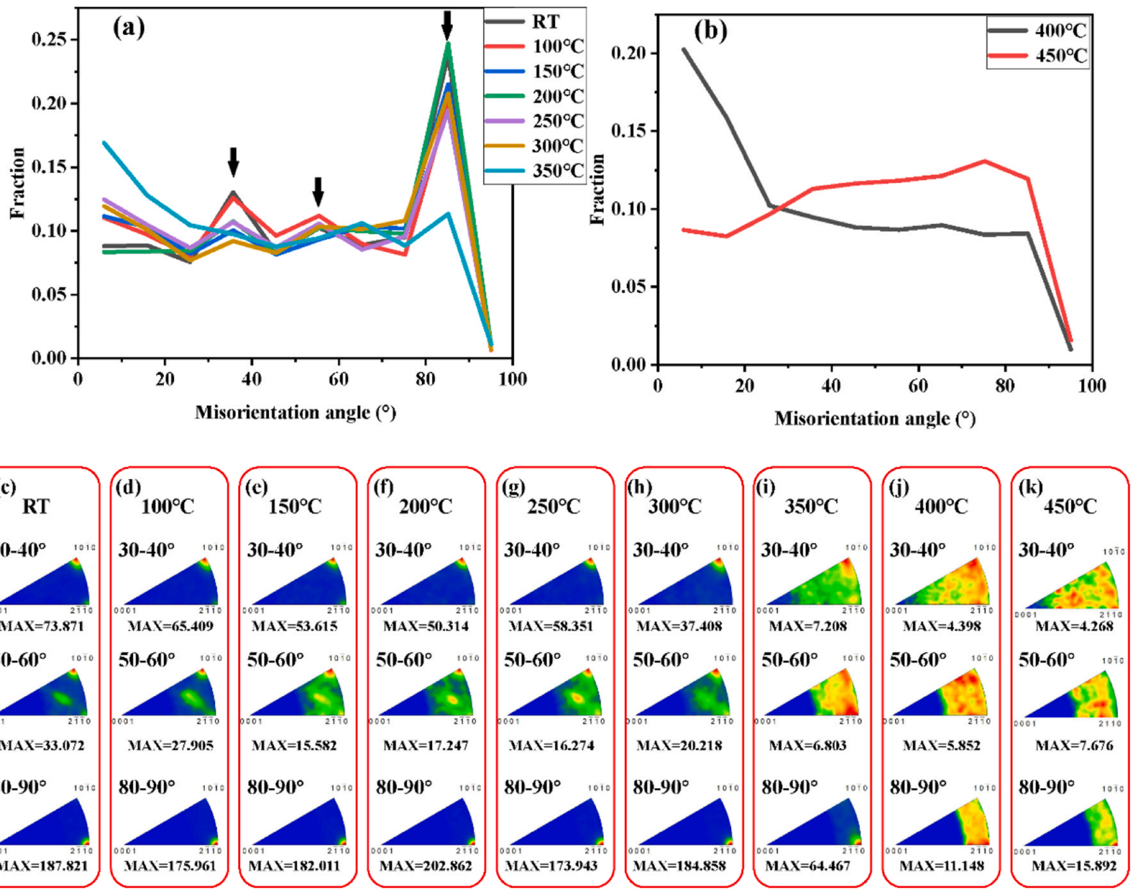

Fig. 4. Misorientation distribution of grain boundaries between identified grains of specimens compressed at (a) RT-350 °C and (b) 400–450 °C. (c–k) Axis/angle distribution of compressed specimens.

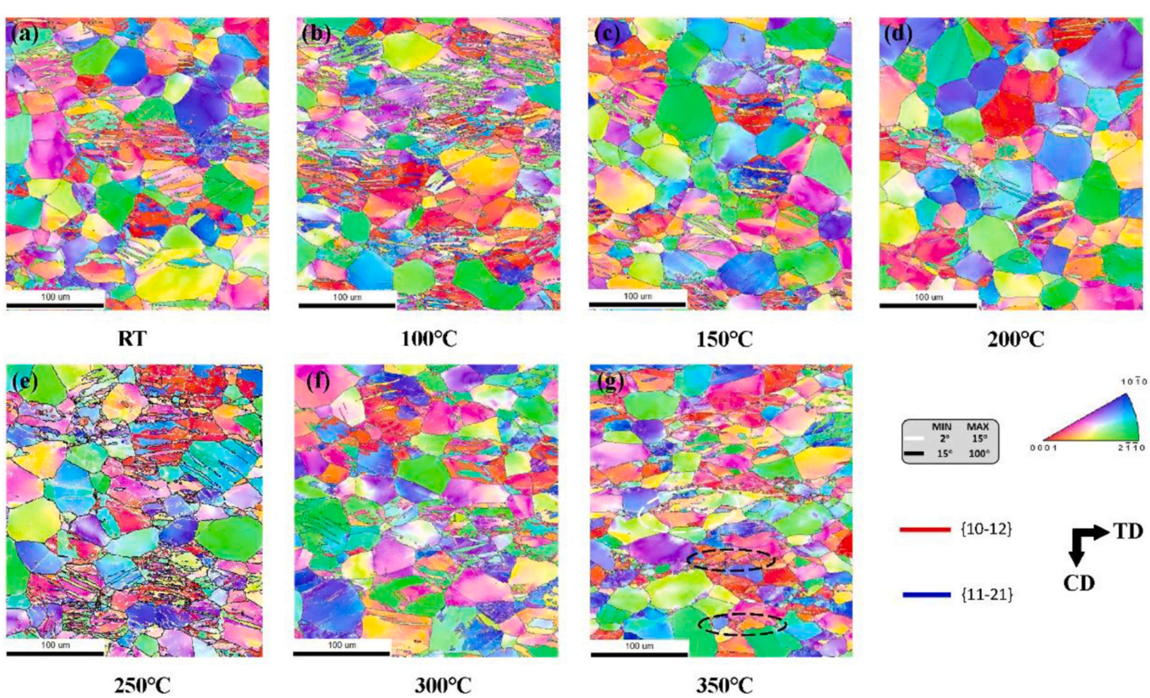

Fig. 5. Inverse pole figure maps of the specimens that compressed at 0–350 °C.

represent twinning behaviors show high values, which indicate high activity of extension twinning. However, the peak values decreased when temperature reached 350 °C and declined further when temperature over 400 °C, which indicate that the twinning activity significantly declined when the temperature reached 350 °C (Fig. 4i) and almost disappeared at the temperature over 400 °C (Fig. 4j–k). Further, there is obviously increasing of LAGBs when compressed at 350–400 °C (Fig. 4a and b), which may indicate the formation of more LAGBs and new grains.

3.3. Microstructure evolution of samples compressed at RT-350 °C

The microstructures of the compressed samples are shown in this section. LAGBs, high angle grain boundaries (HAGBs) and twin boundaries are highlighted as different colors on the inverse pole figure maps. For the convenience of description, grains with <2–1–10> axes approximately parallel to CD were defined as Type 1 while the grains with <10–10> approximately parallel to CD were defined as Type 2.

Partial areas with abundant twin crystals of the specimens compressed at RT-350 °C are shown in Fig. 5 and related boundary maps and partial enlarged areas are shown in Fig. S2. Frequent twin-twin intersections can be observed among all compressed specimens. When compressed at RT-300 °C, large amounts of twin crystals (especially {11−21} twins) with lenticular morphology can be observed and these twin crystals can be rarely seen when the compression temperature increased to 350 °C. The lenticular twin crystals in the specimens compressed at 350 °C exhibit broader morphology compared to that in the specimens compressed at RT-300 °C. When compressed at 350 °C, new grains can be identified, which indicate the occurrence of DRX. Usually, DRX can be classified as continuous dynamic recrystallization (CDRX) and discontinuous dynamic recrystallization (DDRX). CDRX always take place within parent grains, proceeding by recovery progress with the formation of new LAGBs and continuous absorption of dislocations in LAGBs, which finally result in the formation of HAGBs and new grains. DDRX always occurred at grain boundaries, resulting from the serrated boundaries and bugling [26,27]. When compressed at 350 °C, few new grains can be observed forming at parent grain boundaries (indicate by the black circles in Fig. 5g), and the serrated grain boundaries and bulging suggested the occurrence of DDRX. CDRX can also be identified by the formation of LAGBs and new grains within deformed grains (indicate by the white circle in Fig. 5g). Additionally, as shown in Figs. 4 and 5, twinning behaviors become weakened while the fraction of LAGBs increased with the compression temperature increasing and 350 °C is transition temperature, above which the slips will act as the main contributors to accommodate strain. The activity decreasing of {11−21} and {10−12} twinning can be attributed to the competition of other deformation modes. Non-basal slips will activate at high temperature due to the decrease of critical resolved shear stresses (CRSS) and the CRSS of {10−12} twinning always keep low values with the temperature increasing [28,29]. Therefore, 350°C should be the temperature beyond which the CRSS of non-basal slips will be smaller than {11−21} twinning under the deformation condition in this work, which result in the vanishing of {11−21} twin. When the temperature over 400 °C, CRSS of non-basal slip will be smaller than {10−12} twinning, which result in the absence of {10−12} twins. The activity increasing of non-basal can also explain why the LAGBs increased obviously when the compression increasing to 350–400 °C (Fig. 4a, b), because the enhanced <c+a> slip and cross slip are beneficial for the formation of LAGBs and related formation of new grains [30,31].

Two typical grains with Type1 and Type2 orientation were selected out to show the influence of twinning behaviors on texture. As shown in Fig. 6a, two {10−12} twin variants and two {11−21} twin variants can be identified in the grain with Type 1 orientation. Different twin crystals intersected and a large amount of new grain boundaries formed. In the grain with Type 2 orientation (Fig. 6b), only one {10−12} twin variant activated. As mentioned above, the activation of {10−12} and {11−21} twinning behaviors can be dictated by Schmid law and the texture transition were mainly induced by the twinning behaviors (Fig. 3a–n). The grains with Type 1 orientation are beneficial for the activation of {11−21} twinning owing to high Schmid factor and twin-twin intersection between {11−21} and {10−12} twins will restrict the growth of {10−12} twins [15], which result in the residual Type 1 components when compressed at RT-350 °C. In the grains with Type 2 orientation, the <0001> textured parent grains will be greatly consumed by the {10−12} twins owing to the absence of {11−21} twins, thus the Type 2 components became weakened (Fig. 3a–n).

3.4. Microstructure evolution of samples compressed at 400–450 °C

Fig. 7 shows the microstructure of the specimen compressed at 400 °C. Parent grains deformed apparently, and both CDRX and DDRX can be observed while twins can be rarely seen (Fig. 7a). The DRXed grains show chainlike distribution, which usually crossed several parent grains and formed within parent grains and accompanied by LAGBs, thus most of these grain chains that approximately parallel to horizontal direction are identified as CDRXed grains (Fig. 7b). In the grains with <0001> fiber orientation (red color in Fig. 7a), high density of LAGBs and related CDRX can be only seen in partial parent grains, which may indicate that the consumption of parent grains with Type 2 orientation may be induced by the different DRX. Further, the DRXed grains show weak texture (Fig. 7c). Components of <0001>//ED and <10–10>//TD can be identified, which may indicate the emergence of oriented nucleation.

Microstructure of the specimen compressed at 450 °C was shown in Fig. 8. Serrated bugling can be almost observed in all grains, which indicate the activation of DDRX. As shown in Fig. 8a and b, the DRXed grains distribute uniformly within the analyzing area and most of them located in grain boundaries, which indicate the dominant DRX is DDRX. The DRX mechanisms in 400 °C and 450 °C can also be proven by the LAGB decreasing when the compression temperature increasing from 400 °C to 450 °C, because CDRX required more LAGBs within parent grains. Moreover, as reflected in Fig. 8c, the DRXed grains show weak texture with <0001>//CD and <0001>//ED, respectively. Usually, the specific orientation of recrystallized grains usually induced by oriented nucleation [26,32]. In addition, the sizes of DRXed grains when

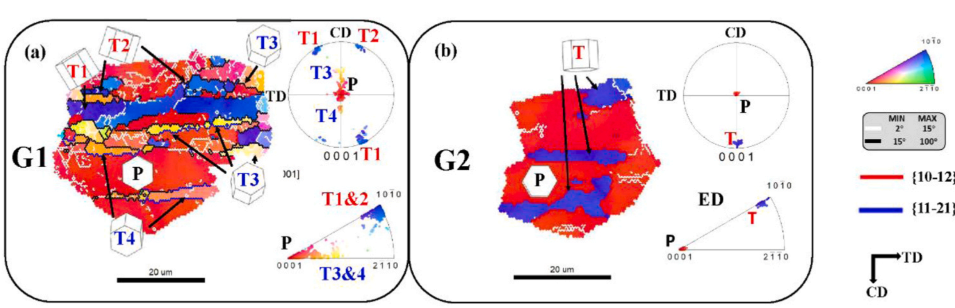

Fig. 6. Grains with (a) Type 1 orientation and (b) Type 2 orientation.

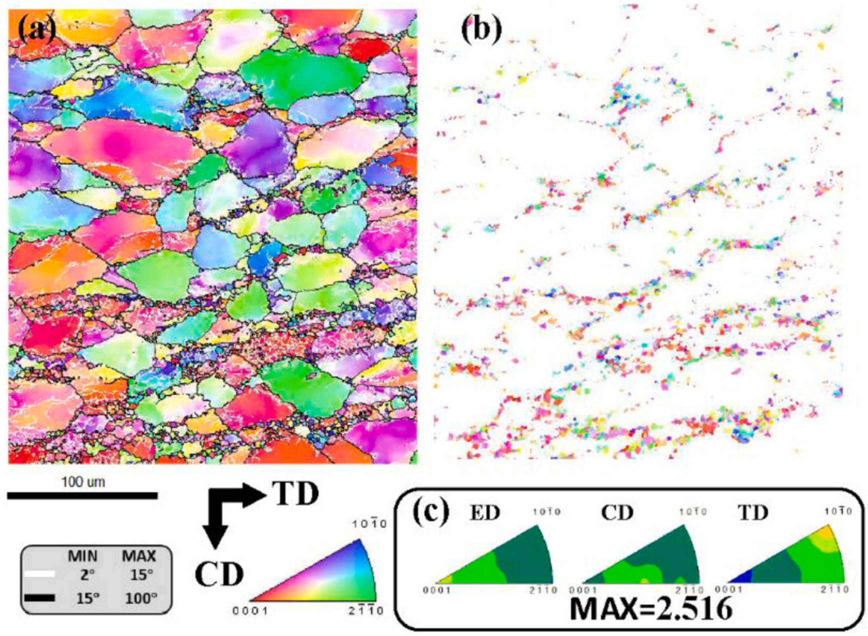

Fig. 7. Microstructure of the specimen compressed at 400 °C. Inverse pole figure maps of (a) selective area with DRX and (b) DRXed grains. (c) Inverse pole figures of DRXed grains in (b).

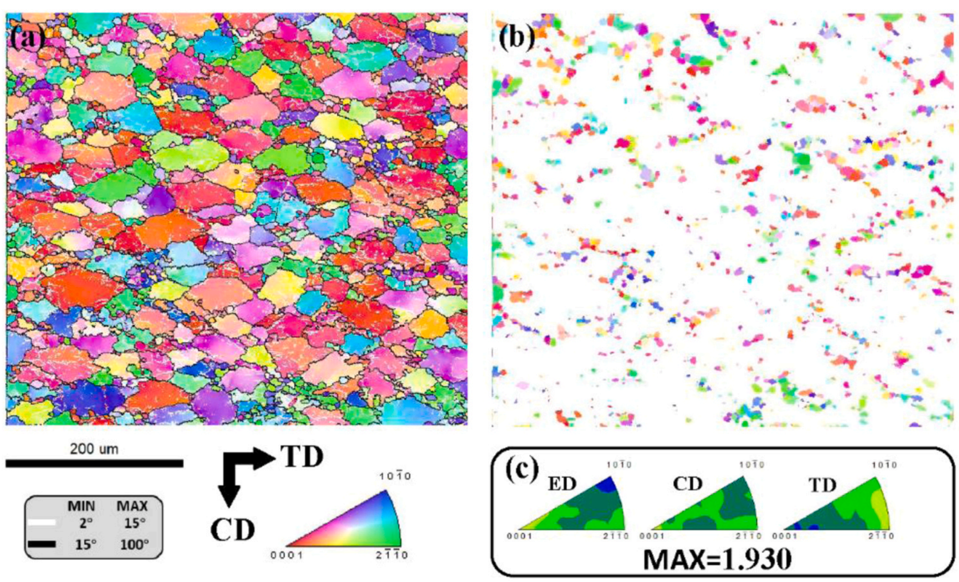

Fig. 8. Microstructure of the specimen compressed at 450 °C. Inverse pole figure maps of (a) selective area with DRX and (b) DRXed grains. (c) Inverse pole figures of DRXed grains in (b).

compressed at 450 °C are obvious larger than that in the sample compressed at 400 °C (Figs. 7b and 8b). Therefore, the preferential grain growth, which will also induce specific texture cannot be ignored [33]. The details will be discussed in Section 4.2.

4. Discussion

4.1. Effects of deformation mechanisms on the formation of Type 1 component

As concluded in Section 3, when compressed at RT-350 °C, the formation of Type 1 components in compressed specimens were mainly caused by twinning-induced consumption of Type 2 components. When compressed at 400–450 °C, texture transitions are mainly induced by DRX. In Mg alloys, DRX is determined by the activated slip modes and related dislocation interaction [34]. Therefore, in Fig. 9, the intragranular misorientation axis analysis (IGMA) was carried out on Type 1 and Type 2 components to analyze the activated dislocation. When compressed at 400 °C (Fig. 9a, c), both the IGMA results of Type 1 and Type 2 show weak pole around <0001> axes, which indicate the activation of prismatic <a> dislocation in residual microstructures [35]. When compressed at 450 °C (Fig. 9b, d), no obvious pole can be seen, which suggest the activation of complex slip modes. Especially, less parent grains can be observed in the residual microstructures with Type 2 orientation, which indicate more active dislocation interaction and resultant formation of grain boundaries and DRXed grains compared to that within Type 1 oriented microstructures.

In order to identify the contribution of slip modes on DRX when

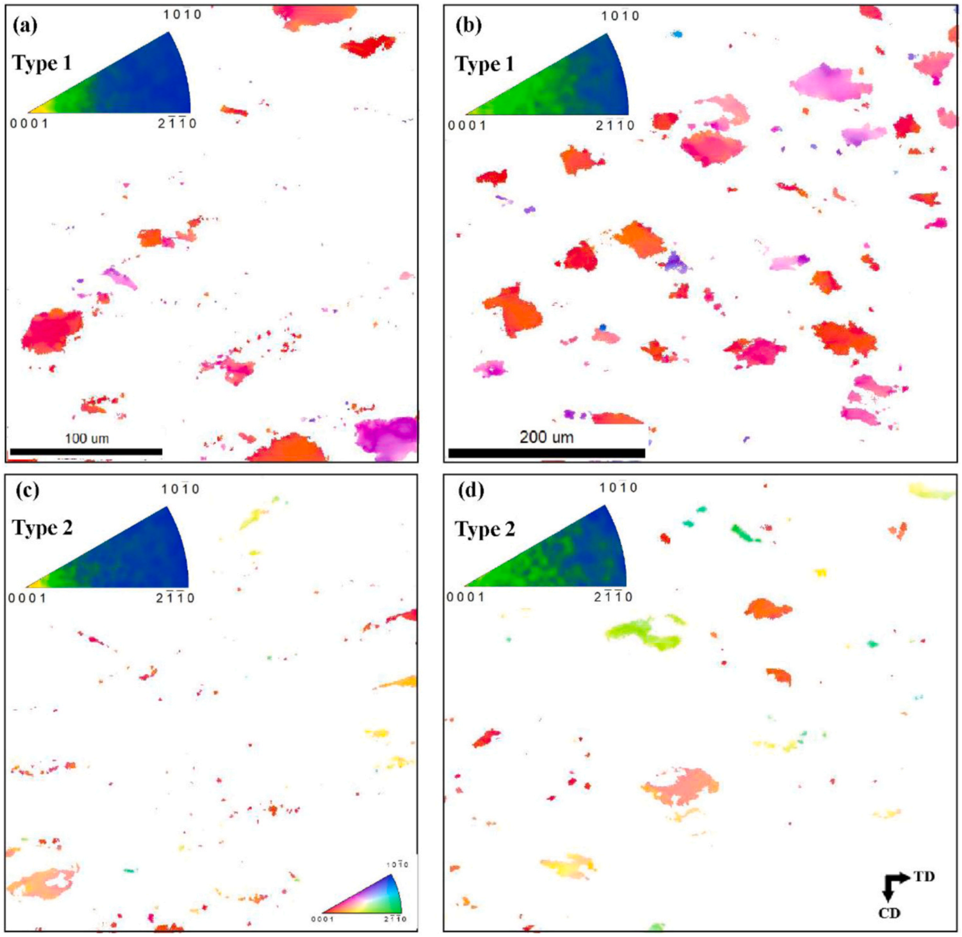

Fig. 9. Inverse pole figure maps and IGMA results of the (a, b) Type 1 and (c, d) Type 2 component when compressed at (a, c) 400 °C and (b, d) 450 °C.

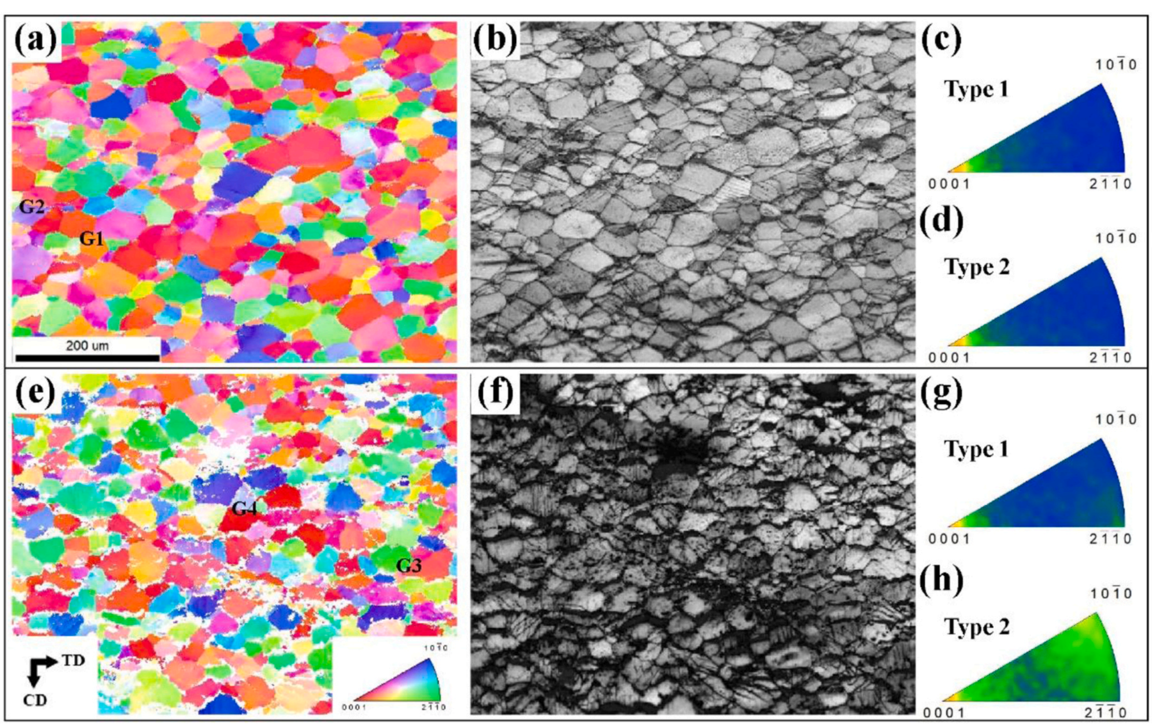

Fig. 10. EBSD results of the cubic specimens compressed at (a-d) 400 °C and (e-h) 450 °C. (a, e) Inverse pole figure maps, (b, f) confidence index maps and IGMA results of microstructure with (c, g) Type 1 and (d, h) Type 2 orientation.

compressed at 400 °C and 450 °C, slip trace analyses and IGMA analyses were conducted on the cubic specimens with the strain of 0.1. DRX can be rarely seen in this stage (Fig. 10a, e) and the optical plane of specimen compressed at 450 °C is rougher compared to that compressed at 400 °C (Fig. 10b, f), which indicate more sever deformation when compressed at 450 °C. Profuse prismatic <a> slip can be identified when compressed at 400 °C in both Type 1 and Type 2 components (Fig. 10c, d). When compressed at 450 °C, more non-prismatic slip can be identified (Fig. 10g, h), which may responsible for the DRX difference of the specimens compressed at 400 °C and 450 °C.

Several grains (G1-G4) with typical orientation were selected from Fig. 10 to analyze the influence of slip on DRX. In G1, massive parallel slip traces can be observed in the grain with Type 1 orientation (Fig. 11a, b), which indicate the activating of frequent slips and most of them are identified as prismatic/pyramidal I slips (Fig. 11c, d). Additionally, there are steps in the center of G1, which suggest the activation of cross-slip [36]. These steps are identified as cross-slip between pyramidal I planes (Fig. 11a, c). In G2, cross-slip can also be recognized by the interaction of slip trace and identified as cross-slip between basal planes and pyramidal I/prismatic planes (Fig. 11e-h). When compressed at 450 °C, in the grain with Type 1 orientation (G3), prismatic <a>/ pyramidal I <c+a> dislocations and related cross-slip can be identified according to the slip trace and IGMA analysis (Fig. 11i-l). In G4 (Fig. 11m-p), cross-slip between pyramidal II/basal planes and prismatic/pyramidal I planes can be identified. In Mg alloys, enhanced <c + a> slip can promote the formation of 3-deminsion dislocation networks, which can drive the recrystallization [16,34]. <c + a> slip can activate easier with the temperature increasing owing to the decline of CRSS [37]. Addition of RE solute is also reported to be beneficial for the activating and stabilizing of <c + a> dislocation [17,18]. Besides, in the matrix with high density of basal <a> and prismatic <a> dislocation, cross-slip and dislocation climb can occur even at RT, which can give rise to the formation of cell wall and sub-grains, finally result in DRX [38,39]. As reflected in Fig. 11, cross-slip between pyramidal planes/prismatic planes can be observed in grains with Type 1 orientation. It is proposed that the addition of RE element can switch primary pyramidal <c + a> dislocations and alter cross-slip, thus pyramidal-to-basal transition and resultant formation of sessile basal-dissociated structure will be restricted, which is beneficial for ductility of Mg alloys [17]. In addition, easier slip transfer condition can be identified according to the nearly parallel slip traces in adjacent grains. Therefore, CDRX in Type 1 oriented microstructure is limited due to the absence of dislocation pinning. In the grains with Type 2 orientation (Fig. 11), the occurrence of cross-slip between basal plane and prismatic/pyramidal planes can create sessile structure [16,40], which will act as obstacle for motion of dislocation during subsequent deformation, thus result in the formation of LAGBs and new grains. In addition, pyramidal II dislocation can also be identified when compressed at 450 °C in Type 2 components, which indicate the enhancement of pyramidal dislocations and related DRX. Therefore, CDRX occurred within grains with Type 2 orientation and consumed the Type 2 components, while the Type 1 component remained in the compressed specimens (Fig. 3).

4.2. Formation of texture of the DRXed grains when compressed above 400 °C

DRXed grains in this work show weak texture. As described in Section 3, when the compression temperature increased from 400 °C to 450 °C, the <0001>//ED components remained while the <0001>//CD component strengthened (Figs. 7c, 8c). In addition, the dominant CDRX

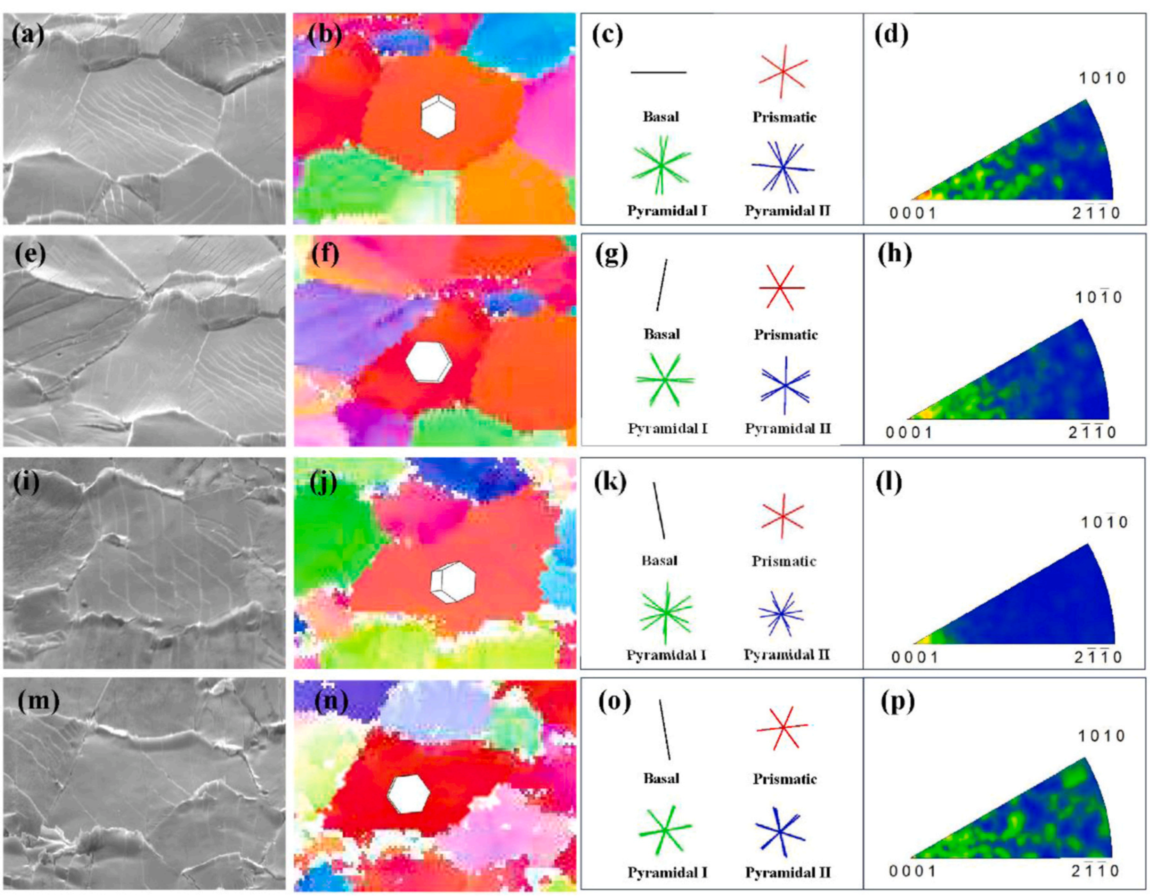

Fig. 11. Slip trace analyses of selective grains (a-d) G1, (e-h) G2, (i-l) G3 and (m-p) G4. (a, e, i, m) SEM images with slip traces, (b, f, j, n) inverse pole figure maps, possible slip traces (c, g, k, o) and (d, h, l, p) IGMA results of selective grains.

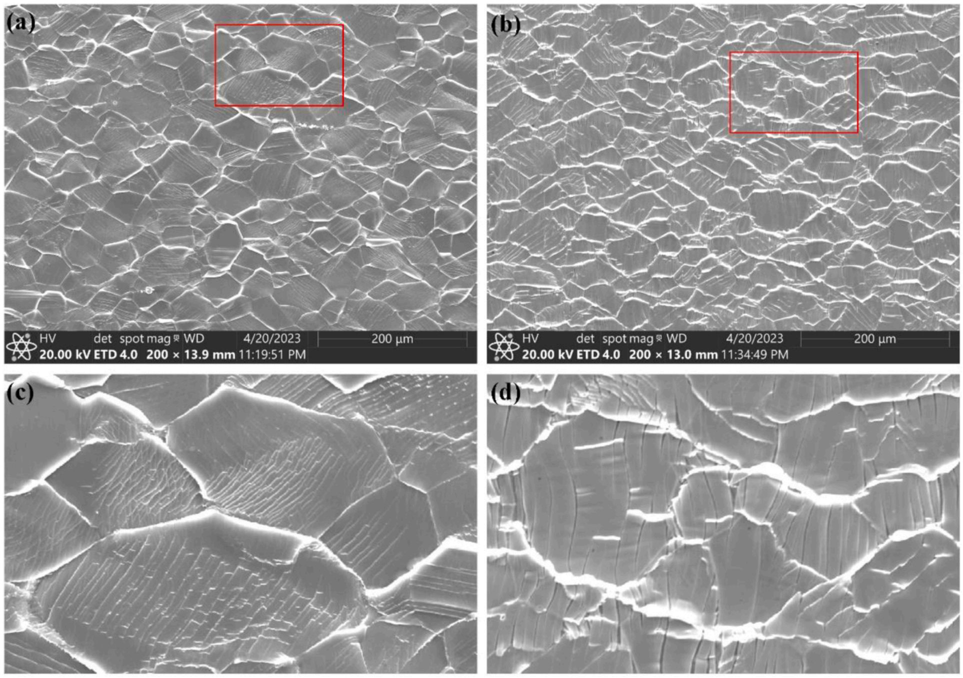

Fig. 12. Slip traces of the cubic sample compressed at (a, c) 400 °C and (b, c) 450 °C and compression tests were interrupted at the strain of 0.2. Selective areas in (a, b) are enlarged and presented in (c, d) to show the slip traces clearly.

turned into DDRX with the temperature increasing (Figs. 7a, 8a). Therefore, it can be inferred that CDRXed grains and DDRXed grains may show different orientations. The slip traces of the samples compressed at 400 °C and 450 °C and interrupted at the strain of 0.2 are shown in Fig. 12. Obviously, the slip trace density of the specimens compressed at 400 °C are higher than that in the specimen compressed at 450 ℃, which indicate more frequent cross slip. Therefore, more sessile structure will be created within grains with Type 1 orientation, which result in the dominant CDRX when compressed at 400 °C (Fig. 7a). When compressed at 450 °C, less slip trace can be observed within parent grains, which indicate less frequency of cross slip. It is proposed that the sessile structure can eliminate gradually with the temperature increasing owing to the dislocation climbing motion [40], thus dislocation accumulation induced by sessile structure pinning will be released and more dislocation will cluster at grain boundaries, which result in the DDRX (Fig. 8a). In addition, as shown in Fig. S3, stress of sample compressed at 450 °C are always lower than that in the sample compressed at 400°C, which indicate more steady flow behaviors. Thus, parent grain boundaries will deform easily when compressed at 450 °C, which is beneficial to DDRX. Obviously, the DRX difference influence the orientation of DRXed grains.

Different DRX mechanisms always result in various orientation of DRXed grains. It is proposed that DDRXed grains always show random orientation, which contribute greatly to texture randomization [26,41,

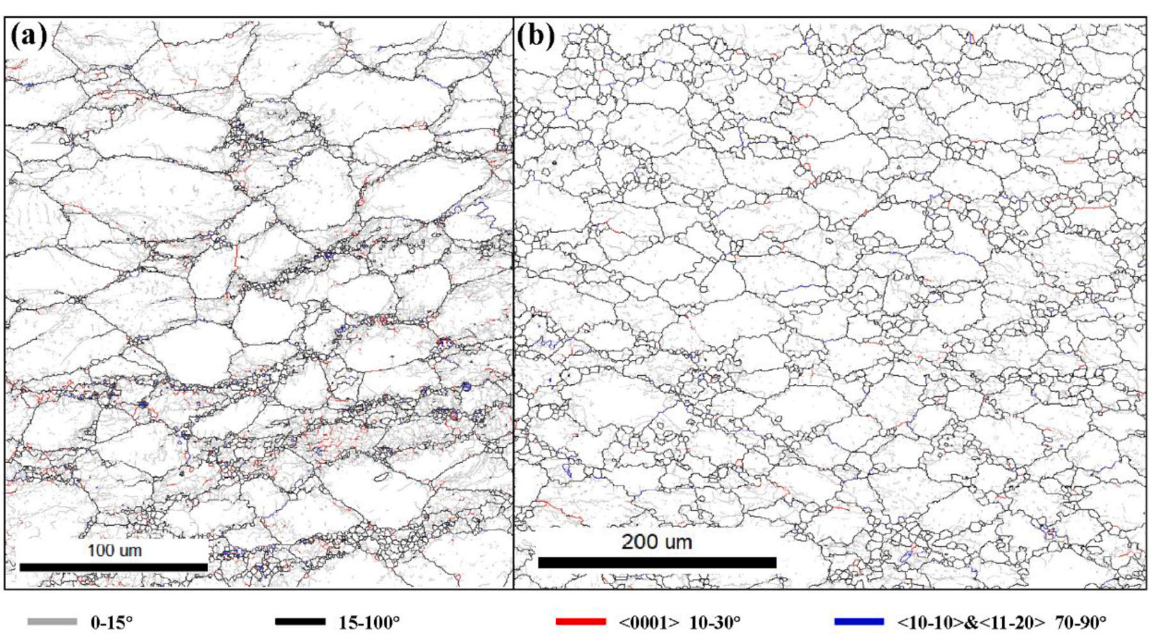

Fig. 13. Grain boundary maps of the specimens compressed at (a) 400 °C and (b) 450 °C.

42]. For CDRXed grains, the new-formed grains are reported to show the orientation that rotate ~30° around <0001> from parent grains [43,44] and its formation had been attributed to the Σ 13a coincident site lattice (CSL) boundaries, which possess low interfacial energy and high mobility [44–46]. As shown in Fig. 13a, when compressed at 400 °C, massive grain boundaries with misorientation angle of 5–30° and rotation axes of <0001> and resultant CDRX can be observed within parent grains, which is responsible for the formation of <0001>//ED component. In addition, grain boundaries with rotation angle of 70–90° and related DDRX can be observed formed at the grain boundaries and the growth of DDRXed grains may result in the formation of <0001>//CD components in the specimens compressed at 450 °C. As mentioned above, when compressed at 450 °C, DDRX predominate DRX behaviors. Some Near-CSL boundaries, i.e., Σ 17a (83.63°, <2–1–10>) are proposed to show high mobility [47,48]. The grain with Type 2 orientation will also show high storage energy owing to the formation of more sessile structure that induced by cross-slip. Therefore, the DDRXed grains which share specific grain boundaries will swallow the parent grains with Type 2 orientation owing to the high storage energy of parent grains and result in the <0001>//CD component. When compressed at 450 °C, DDRX become dominant, thus <0001>//CD component was strengthened.

5. Conclusions

In summary, twinning behaviors and DRX of <0001> textured Mg-17.5Gd-Zr (wt%) alloy were systemically investigate through compression. The influence of temperature on deformation modes and related microstructure and texture transition were analyzed. The main conclusions are summarized as follows:

(1) After compression, <10–10>//CD component was consumed, which result in the formation of <2–1–10>//ED component in the compressed samples. Both twinning behaviors and DRX consume the <10–10>//CD component preferentially.

(2) When compressed at RT-350 °C, {10−12} and {11−21} twinning behaviors show high activity and act as the main contributors to the consumption of <10–10>//CD oriented microstructure. Both {10−12} and {11−21} twinning behaviors at this temperature range can be governed by Schmid law.

(3) When compressed at 400–450 °C, DRX are responsible for the formation of <2–1–10>//ED orientation by consuming the <10–10>//CD oriented components. The dominate DRX changed from CDRX to DDRX with the temperature increasing.

(4) CDRX are mainly induced by the formation of sessile structure which originate from the cross-slip between non-basal plane and basal plane. With temperature increasing, the elimination of sessile structure is considered to be the main contributor to the transition from CDRX to DDRX.

(5) The <0001>//ED components in DRXed grains are induced by the CDRX, which result from the formation of Σ 13a near-CSL boundaries. The <0001>//CD are mainly induced by the high mobility of near-CSL boundaries, i.e., Σ 17a (83.63°, <2–1–10>) between DDRXed grains and parent grains with <10–10>//CD orientation.

CRediT authorship contribution statement

Zhiwei Shan: Supervision, Data curation. **Rongshi Chen:** Supervision, Resources, Funding acquisition. **Boyu Liu:** Supervision, Data curation. **Hong Yan:** Supervision, Funding acquisition. **Lingyu Zhao:** Writing – review & editing, Validation, Supervision, Methodology. **Ning Lv:** Writing – review & editing, Writing – original draft, Software, Methodology, Conceptualization.

Declaration of Competing Interest

The authors declare that they have no known competing financial interests or personal relationships that could have appeared to influence the work reported in this paper

Acknowledgements

This work was financially supported by the National Natural Science Foundation of China (Nos. 52301164, 52371121 and 52271107), Natural Science Foundation of Shandong Province (No. ZR2021ME241), the Basic Research Project of Education Department of Liaoning Province (JYTQN2023066).

Appendix A. Supporting information

Supplementary data associated with this article can be found in the online version at doi:10.1016/j.jallcom.2024.177299.

Data availability

Data will be made available on request.

References

[1] S.V.S. Prasad, S.B. Prasad, K. Verma, R.K. Mishra, V. Kumar, S. Singh, The role and significance of Magnesium in modern day research-a review, J. Mag. Alloy. 10 (1) (2022) 1–61, https://doi.org/10.1016/j.jma.2021.05.012.

[2] X. Peng, W. Liu, G. Wu, H. Ji, W. Ding, Plastic deformation and heat treatment of Mg-Li alloys: a review, J. Mater. Sci. Technol. 99 (2022) 193–206, https://doi.org/10.1016/j.jmst.2021.04.072.

[3] Y. Yang, X. Xiong, J. Chen, X. Peng, D. Chen, F. Pan, Research advances of magnesium and magnesium alloys worldwide in 2022, J. Mag. Alloy. 11 (8) (2023) 2611–2654, https://doi.org/10.1016/j.jma.2023.07.011.

[4] J. Zhang, J. Miao, N. Balasubramani, D.H. Cho, T. Avey, C.-Y. Chang, A.A. Luo, Magnesium research and applications: Past, present and future, J. Mag. Alloy. 11 (11) (2023) 3867–3895, https://doi.org/10.1016/j.jma.2023.11.007.

[5] H. Yan, X.H. Shao, H.P. Li, R.S. Chen, H.Z. Cui, E.-H. Han, Synergization of ductility and yield strength in a dilute quaternary Mg-Zn-Gd-Ca alloy through texture modification and Guinier-Preston zone, Scr. Mater. 207 (2022), https://doi.org/10.1016/j.scriptamat.2021.114257.

[6] M.G. Jiang, C. Xu, T. Nakata, H. Yan, R.S. Chen, S. Kamado, Rare earth texture and improved ductility in a Mg-Zn-Gd alloy after high-speed extrusion, Mater. Sci. Eng. A-Struct. Mater. Prop. Microstruct. Process. 667 (2016) 233–239, https://doi.org/10.1016/j.msea.2016.04.093.

[7] M.G. Jiang, C. Xu, T. Nakata, H. Yan, R.S. Chen, S. Kamado, Enhancing strength and ductility of Mg-Zn-Gd alloy via slow-speed extrusion combined with pre-forging, J. Alloy. Compd. 694 (2017) 1214–1223, https://doi.org/10.1016/j.jallcom.2016.10.109.

[8] H. Yan, S.W. Xu, R.S. Chen, S. Kamado, T. Honma, E.H. Han, Activation of {10(1) over-bar2} twinning and slip in high ductile Mg-2.0Zn-0.8Gd rolled sheet with non-basal texture during tensile deformation at room temperature, J. Alloy. Compd. 566 (2013) 98–107, https://doi.org/10.1016/j.jallcom.2013.03.008.

[9] Z. Yu, Y. Huang, X. Qiu, G. Wang, F. Meng, N. Hort, J. Meng, Fabrication of a high strength Mg–11Gd–4.5Y–1Nd–1.5Zn–0.5Zr (wt%) alloy by thermomechanical treatments, Mater. Sci. Eng. A. 622 (2015) 121–130, https://doi.org/10.1016/j.msea.2014.10.077.

[10] Z. Yu, C. Xu, J. Meng, S. Kamado, Microstructure evolution and mechanical properties of a high strength Mg-11.7Gd-4.9Y-0.3Zr (wt%) alloy prepared by pre-deformation annealing, hot extrusion and ageing, Mater. Sci. Eng. A 703 (2017) 348–358, https://doi.org/10.1016/j.msea.2017.06.096.

[11] N. Stanford, R.K.W. Marceau, M.R. Barnett, The effect of high yttrium solute concentration on the twinning behaviour of magnesium alloys, Acta Mater. 82 (2015) 447–456, https://doi.org/10.1016/j.actamat.2014.09.022.

[12] J. Li, Z. Dong, X. Yi, D. Wu, R. Chen, Twin evolution in cast Mg-Gd-Y alloys and its dependence on aging heat treatment, J. Mag. Alloy. 11 (7) (2023) 2285–2298, https://doi.org/10.1016/j.jma.2021.09.023.

[13] Q. Zhang, T.-W. Fan, L. Fu, B.-Y. Tang, L.-M. Peng, W.-J. Ding, Ab-initio study of the effect of rare-earth elements on the stacking faults of Mg solid solutions, Intermetallics 29 (2012) 21–26, https://doi.org/10.1016/j.intermet.2012.04.015.

[14] S.R. Agnew, L. Capolungo, C.A. Calhoun, Connections between the basal I1 "growth" fault and ⟨c+a⟩ dislocations, Acta Mater. 82 (2015) 255–265, https://doi.org/10.1016/j.actamat.2014.07.056.

[15] N. Lv, L. Zhao, H. Yan, B. Liu, R. Chen, Z. Shan, Anomalous ductility-strength synergy occurred after cold rolling in a high Gd content Mg alloy, J. Mater. Sci. Technol. 207 (2025) 177–190, https://doi.org/10.1016/j.jmst.2024.03.076.

[16] Z. Wu, R. Ahmad, B. Yin, S. Sandlöbes, W.A. Curtin, Mechanistic origin and predictionof enhanced ductility inmagnesium alloys, Science 359 (2018) 447–452, https://doi.org/10.1126/science.aap8716.

[17] R. Ahmad, Z. Wu, W.A. Curtin, Analysis of double cross-slip of pyramidal I ⟨c+a⟩ screw dislocations and implications for ductility in Mg alloys, Acta Mater. 183 (2020) 228–241, https://doi.org/10.1016/j.actamat.2019.10.053.

[18] S. Sandlöbes, M. Friák, S. Zaefferer, A. Dick, S. Yi, D. Letzig, Z. Pei, L.F. Zhu, J. Neugebauer, D. Raabe, The relation between ductility and stacking fault energies in Mg and Mg–Y alloys, Acta Mater. 60 (6-7) (2012) 3011–3021, https://doi.org/10.1016/j.actamat.2012.02.006.

[19] K.D. Molodov, T. Al-Samman, D.A. Molodov, Effect of gadolinium on the deformation and recrystallization behavior of magnesium crystals, Acta Mater. 240 (2022), https://doi.org/10.1016/j.actamat.2022.118312.

[20] N. Lv, L. Zhao, H. Yan, B. Liu, Y. Mao, Z. Shan, R. Chen, Texture tailoring and microstructure refinement induced by {11−21} and {10−12} twinning in an extruded Mg-Gd alloy, J. Alloy. Compd. 966 (2023), https://doi.org/10.1016/j.jallcom.2023.171590.

[21] Z. Zeng, N. Stanford, C.H.J. Davies, J.-F. Nie, N. Birbilis, Magnesium extrusion alloys: a review of developments and prospects, Int. Mater. Rev. 64 (1) (2018) 27–62, https://doi.org/10.1080/09506608.2017.1421439.

[22] R.G. Li, D.Y. Zhao, J.H. Zhang, H.R. Li, Y.Q. Dai, D.Q. Fang, Room temperature yielding phenomenon in extruded or/and aged Mg-14Gd-2Ag-0.5Zr alloy with fine-grained microstructure, Mater. Sci. Eng. A. 787 (2020), https://doi.org/10.1016/j.msea.2020.139551.

[23] J. Zheng, Z. Chen, Z. Yan, Z. Zhang, Q. Wang, Y. Xue, Preparation of ultra-high strength Mg-Gd-Y-Zn-Zr alloy by pre-ageing treatment prior to extrusion, J. Alloy. Compd. 894 (2022), https://doi.org/10.1016/j.jallcom.2021.162490.

[24] S.-H. Kim, J.-G. Jung, B.S. You, S.H. Park, Microstructure and texture variation with Gd addition in extruded magnesium, J. Alloy. Compd. 695 (2017) 344–350, https://doi.org/10.1016/j.jallcom.2016.10.179.

[25] X. Wang, Y. Yu, W. Chen, X. Zhang, D. Fang, W. Zhang, W. Wang, Formation mechanism of <0001> texture connected with excellent ductility during hot extrusion in Mg-9Gd-5Y-0.5Zr alloy, Mater. Sci. Eng. A. 859 (2022), https://doi.org/10.1016/j.msea.2022.144193.

[26] M.G. Jiang, C. Xu, H. Yan, G.H. Fan, T. Nakata, C.S. Lao, R.S. Chen, S. Kamado, E. H. Han, B.H. Lu, Unveiling the formation of basal texture variations based on twinning and dynamic recrystallization in AZ31 magnesium alloy during extrusion, Acta Mater. 157 (2018) 53–71, https://doi.org/10.1016/j.actamat.2018.07.014.

[27] K. Huang, R.E. Logé, A review of dynamic recrystallization phenomena in metallic materials, Mater. Des. 111 (2016) 548–574, https://doi.org/10.1016/j.matdes.2016.09.012.

[28] H. Fan, Q. Wang, X. Tian, J.A. El-Awady, Temperature effects on the mobility of pyramidal $< c + a >$ dislocations in magnesium, Scr. Mater. 127 (2017) 68–71, https://doi.org/10.1016/j.scriptamat.2016.09.002.

[29] A. Chapuis, J.H. Driver, Temperature dependency of slip and twinning in plane strain compressed magnesium single crystals, Acta Mater. 59 (5) (2011) 1986–1994, https://doi.org/10.1016/j.actamat.2010.11.064.

[30] A. Galiyev, R. Kaibyshev, G. Gottstein, Correlation of plastic deformation and dynamic recrystallization in magnesium alloy ZK60, Acta Mater. 49 (7) (2001) 1199–1207, https://doi.org/10.1016/S1359-6454(01)00020-9.

[31] Z. Wu, R. Ahmad, Mechanistic origin and predictionof enhanced ductility inmagnesium alloys, Science 359 (2018) 447–452, https://doi.org/10.1126/science.aap8716.

[32] L.Y. Zhao, H. Yan, R.S. Chen, E.-H. Han, Oriented nucleation causing unusual texture transition during static recrystallization annealing in cold-rolled Mg–Zn–Gd alloys, Scr. Mater. 188 (2020) 200–205, https://doi.org/10.1016/j.scriptamat.2020.07.037.

[33] M.G. Jiang, C. Xu, H. Yan, T. Nakata, Z.W. Chen, C.S. Lao, R.S. Chen, S. Kamado, E. H. Han, Quasi-in-situ observing the rare earth texture evolution in an extruded Mg-Zn-Gd alloy with bimodal microstructure, J. Mag. Alloy. 9 (5) (2021) 1797–1805, https://doi.org/10.1016/j.jma.2020.09.001.

[34] A. Galiyev, R. Kaibyshev, G. Gottstein, Correlation of plastic deformation and dynamic recrystallization in magnesium alloy ZK60, Acta Mater. 49 (2001) 1109–1207, https://doi.org/10.1016/S1359-6454(01)00020-9.

[35] M. Yamasaki, K. Hagihara, S.-i Inoue, J.P. Hadorn, Y. Kawamura, Crystallographic classification of kink bands in an extruded Mg–Zn–Y alloy using intragranular misorientation axis analysis, Acta Mater. 61 (6) (2013) 2065–2076, https://doi.org/10.1016/j.actamat.2012.12.026.

[36] D.F. Shi, A. Ma, M.T. Pérez-Prado, C.M. Cepeda-Jiménez, Activation of second-order <c+a> pyramidal slip and other secondary mechanisms in solid solution Mg-Zn alloys and their effect on tensile ductility, Acta Mater. 244 (2023), https://doi.org/10.1016/j.actamat.2022.118555.

[37] A. Chapuis, Q. Liu, Investigating the temperature dependency of plastic deformation in a Mg-3Al-1Zn alloy, Mater. Sci. Eng. A 725 (2018) 108–118, https://doi.org/10.1016/j.msea.2018.04.019.

[38] I. Basu, T. Al-Samman, Twin recrystallization mechanisms in magnesium-rare earth alloys, Acta Mater. 96 (2015) 111–132, https://doi.org/10.1016/j.actamat.2015.05.044.

[39] K.D. Molodov, T. Al-Samman, D.A. Molodov, G. Gottstein, Mechanisms of exceptional ductility of magnesium single crystal during deformation at room temperature: multiple twinning and dynamic recrystallization, Acta Mater. 76 (2014) 314–330, https://doi.org/10.1016/j.actamat.2014.04.066.

[40] K. Takagi, M. Yamasaki, Y. Mine, K. Takashima, Temperature dependence of prismatic slip in a single-crystalline long-period stacking ordered Mg–Zn–Y alloy, Scr. Mater. 178 (2020) 498–502, https://doi.org/10.1016/j.scriptamat.2019.12.025.

[41] M.R. Barnett, A. Sullivan, N. Stanford, N. Ross, A. Beer, Texture selection mechanisms in uniaxially extruded magnesium alloys, Scr. Mater. 63 (7) (2010) 721–724, https://doi.org/10.1016/j.scriptamat.2010.01.018.

[42] M.G. Jiang, H. Yan, R.S. Chen, Twinning, recrystallization and texture development during multi-directional impact forging in an AZ61 Mg alloy, J. Alloy. Compd. 650 (2015) 399–409, https://doi.org/10.1016/j.jallcom.2015.07.281.

[43] P. Šedá, A. Jäger, P. Lejček, P. Romano Triguero, Formation of grain boundaries in magnesium single crystal during equal channel angular pressing, Philos. Mag. 94 (10) (2014) 1095–1111, https://doi.org/10.1080/14786435.2013.878050.

[44] M.G. Jiang, C. Xu, H. Yan, S.H. Lu, T. Nakata, C.S. Lao, R.S. Chen, S. Kamado, E. H. Han, Correlation between dynamic recrystallization and formation of rare earth texture in a Mg-Zn-Gd magnesium alloy during extrusion, Sci. Rep. 8 (1) (2018), https://doi.org/10.1038/s41598-018-35170-4.

[45] C.D. Barrett, A. Imandoust, A.L. Oppedal, K. Inal, M.A. Tschopp, H. El Kadiri, Effect of grain boundaries on texture formation during dynamic recrystallization of magnesium alloys, Acta Mater. 128 (2017) 270–283, https://doi.org/10.1016/j.actamat.2017.01.063.

[46] X. Liu, J. Wang, Low-energy, Mobile grain boundaries in magnesium, Sci. Rep. 6 (1) (2016), https://doi.org/10.1038/srep21393.

[47] N. Lv, L. Zhao, H. Yan, B. Liu, R. Chen, Z. Shan, Unusual twin induced recrystallization and corresponding texture optimization in a cold rolled Mg-Gd-Zr alloy during annealing, J. Mag. Alloy. (2024), https://doi.org/10.1016/j.jma.2024.04.015.

[48] L.Y. Zhao, H. Yan, R.S. Chen, E.-H. Han, The preferential growth and related textural evolution during static recrystallization in a cold-rolled Mg-Zn-Gd alloy, J. Mag. Alloy 9 (3) (2021) 818–828, https://doi.org/10.1016/j.jma.2020.02.026.